Proc. Estonian Acad. Sci. Eng., 2006, **12**, 2, 96–110

Investigation of solid hybrid solar cells based on molecular glasses

Fabrice Goubard[a], Reda Aîch[a,d], François Tran-Van[a], Asta Michaleviciute[b], Franck Wünsch[c], Marinus Kunst[c], Josas Grazulevicius[b], Bernard Ratier[e] and Claude Chevrot[a]

[a] Laboratoire de Physicochimie des Polymères et des Interfaces (EA 2528), Université de Cergy-Pontoise, 5 mail Gay Lussac, 95013 Cergy Pontoise, France; fabrice.goubard@chim.u-cergy.fr
[b] Department of Organic Technology, Kaunas University of Technology, Radvilenu Plentas 19, Kaunas 3028, Lithuania
[c] Hahn-Meitner-Institut, Bereich Solare Energetik, Glienickerstrasse 100, 14109 Berlin, Germany
[d] Ecole Electricité de Production et Méthodes Industrielles, 13 bd de l'Hautil, 95092 Cergy Pontoise, France
[e] UMOP/OCMP, FRE-CNRS 2701, Faculté des Sciences et Techniques, avenue Albert Thomas, 87060 Limoges, France

Received 7 November 2005, in revised form 10 January 2006

Abstract. We have synthesized new carbazole and ethylenedioxythiophene based molecular glasses with hydrazone and imine goups. Thermal analysis confirms the metastable amorphous properties of these molecules with glass temperature in the range of 62 to 76 °C. Electrochemical properties have been studied and show the effect of the conjugated imine or hydrazone groups on the electronic delocalization of the structures. A decrease of the oxidation potential, compared to the parent unsubstituted molecules, is observed, which decreases the HOMO energetic level and improves the donor properties of the molecules. Amorphous materials of low molecular weight should allow the regeneration of the oxidized sensitizer in agreement with their respective energetic levels. Moreover, all the molecules absorb light in the range of the wavelength, blue-shifted in comparison with the ruthenium dye, which limits the shield effect for a good photogeneration of charge carrier in the dye. Results suggest that such molecular glasses could find applications in photovoltaic devices.

Key words: molecular glasses, photovoltaic cells, TiO_2, hybrid materials, TRMC experiments.

1. INTRODUCTION

Although the dye-sensitized TiO_2 nanocrystalline photoelectrochemical solar cells show excellent power conversion performance (about 10%) [1–3], their commercial application is still limited due to the instability of the cell (like

evaporation of the electrolyte and degradation of the electrolyte or of the dye) as well as to technological aspects of the large module production, using a liquid electrolyte.

Various approaches have been reported in the literature for the replacement of the liquid electrolyte like a polymer gel electrolyte that conducts ions [4], inorganic materials such as *p*-type CuI or CuSCN, as well as organic hole conductors such as triphenyldiamine (TPD) polypyrrole [5–9]. Bach et al. [10] used an amorphous organic hole transport material (HTM) to replace the electrolyte, in which positive charges are transported by hopping processes. Furthermore, *p*-type semiconducting polymers that accept holes from the dye are potential candidates for replacing the liquid electrolytes [5–8,10]. In order to realize solid state cells, several requirements have to be fulfilled [11]. Insertion of low molecular weight molecules acts as holes acceptor and transport layer in the porosity of dye-sensitized nanocrystalline TiO_2 (nc-TiO_2) and will allow an optimized *n-p* heterojunction in comparison with conjugated polymers such as polypyrrole or polythiophene derivatives [12,13]. Molecular glasses (amorphous molecular materials) are defined as low-molecular weight compounds, which can exist in a glassy state at ambient temperature and form solid amorphous films on a substrate [14]. In such a multilayer device, the molecular glasses fulfil the combined function of the hole acceptor and hole transport layer.

In this work, we have studied carbazole and 3,4-ethylenedioxythiophene derivatives containing hydrazone (HY-CARB) or imine structures (CARB-I-CARB and CARB-I-EDOT) with properties of molecular glasses, donor properties, good hole mobility and no absorption in the range of the sensitizer. We will present one example of hybrid photovoltaic devices, based on the following composite: SnO_2:F/nc-TiO_2/Ru-dye/HY-CARB/Au. Characteristics of each layer in terms of charge transport are discussed.

2. EXPERIMENTAL

We realized devices, constituted of 1) a transparent and conductive SnO_2 (FTO) layer, 2) a dense film and a porous film of TiO_2 semiconductor nano-particles (electron acceptor and transport layer), spin-coated onto the FTO substrate, 3) a monolayer of a Ruthenium-bipyridil-based dye for light absorption and electron injection into the TiO_2 conduction band and 4) a molecular glass of hydrazone structure used as the acceptor of holes and a transport layer, covered by a thin layer of gold.

All devices were produced on 1×1 cm transparent conducting oxide (fluorine doped) tin oxide (SnO_2:F) covered glass substrates with an active area of 5 mm^2. Figure 1a shows the configuration of a hybrid solid-state solar cell together with the chemical structures of the materials used.

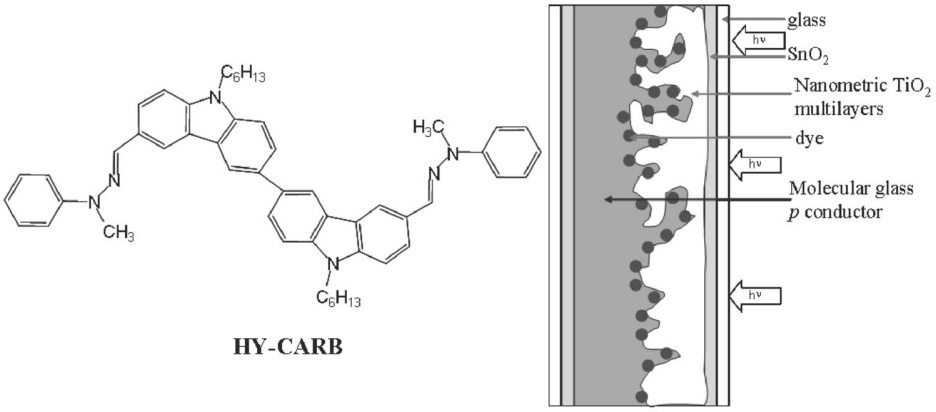

(a)

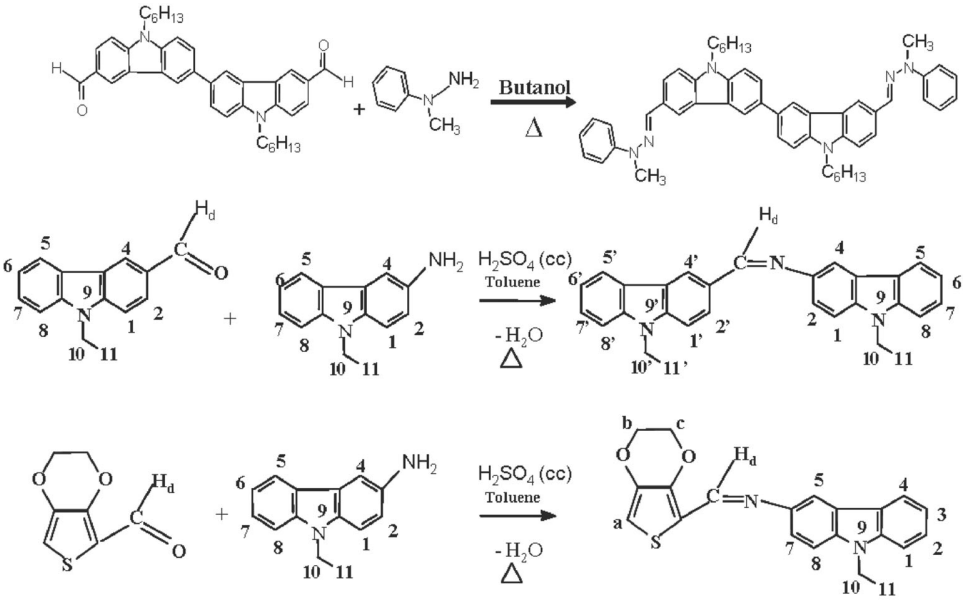

(b)

Fig. 1. Schematic diagram of the device (a) and a schematic of the synthesis (b).

2.1. Synthesis of molecular glasses

HY-CARB is prepared in a synthetic way by first formylation of the N-hexylcarbazole or 3,4-ethylenedioxythiophene by a Vielsmeier method and then condensation of the aldehyde with substituted hydrazine in butanol as already described in [15].

2.1.1. Synthesis of [1-(2,3-dihydrothienol[3,4-b][1,4]dioxin-5-yl)-meth-(E)-ylidene]-(9-ethylcarbazole-3-yl)amine (CARB-I-EDOT)

In a 100 ml two-neck round bottom flask, fitted with a reflux condenser and a Dean-Stark apparatus, 1 g (5.88 mmol) of 2-(3,4-ethylenedioxythiophene) carboxaldehyde and 2.94 g (13.98 mmol) of 3-amino-N-ethylcarbazole are solubilized in 50 ml of toluene. The solution is acidified with H_2SO_4 and maintained at reflux during 16 h. After cooling and filtration, the solution is evaporated under vacuum to obtain a brown solid. The crude product is then washed with 100 ml of boiling methanol and after filtration the insoluble is recristallized in 60 ml of propanol (yield 63%).
RMN ^{1}H (250 MHz, $CDCl_3$) (δ ppm): 8.74 (s, H, (H_4,)), 8.06 (d, H, (H_2)), 7.99 (s, H, (H_d)), 7.41 (m, 4H, ($H_{1,6,7,8}$)), 7.20 (d, 1H, (H_5)), 6.51 (s, 1H (H_a)), 4.37–4.27 (m,6H,($2H_{b'}$ $2H_{c'}$ $2H_{10}$)), 1.45 (t,3H,(H_{11})

2.1.2. Synthesis of (9-ethylcarbazole-3-yl)-[1-(9-ethylcarbazole-3-yl)-meth-(E)-ylidene amine (CARB-I-CARB)

In a 100 ml two-neck round bottom flask, fitted with a reflux condenser and a Dean-Stark apparatus, 2 g (8.95 mmol) of N-ethylcarbazole 3-carboxaldehyde and 1.88 g (8.95 mmol) of 3-amino-N-ethylcarbazole are solubilized in 50 ml of toluene. After acidification with H_2SO_4, the solution is refluxed during 16 h. After cooling, the crude product is precipitated and then filtrated. After the first recristallization in propanol, the product is purified a second time by silica gel column chromatography using ether as eluent; 2.34 g of pale yellow cristals are obtained (yield 62%).
RMN ^{1}H (250 MHz, $CDCl_3$) (ppm): 8.80(s,1H,(H_d),8.67(s,1H,(H_4),8.15(m,3H, ($H_{2,2'}$, H_1)), 8.05(s,1H,($H_{4'}$),7.50(m,7H,($H_{1'}$,$H_{8,8'}$, $H_{6,6'}$, $H_{7,7'}$)
7.25(m,2H,($H_{5,5'}$)),4.35(m,4H,($H_{10,10'}$)),1.70-1.45(m,6H,($H_{11,11'}$))

Absorption spectra were measured with a UV-Vis spectrophometer (U-570 JASCO). Electrochemical measurements were carried out using an EG & G PAR 273 potentiostat-galvanostat in a three-electrode single-compartment cell. The working electrode was a platinum disc (diameter 1 cm). The counter electrode was a platinum wire. The reference electrode was a saturated calomel electrode for all the electrochemical experiments with a salt bridge containing the supporting electrolyte. Cyclic voltammetry was performed in CH_3CN + 0.1 M lithium perchlorate solution.

UV-VIS spectra were obtained from a JASCO V-570 spectrophotometer at 400 nm/min (bandwidth 2 nm).

2.2. Preparation of mesoporous nanocrystalline TiO_2 films

Dense films of TiO_2 were deposited on fluorine-doped conducting tin oxide glasses (sheet resistance about 15 Ω/sq) by the following method. Prior to use, FTO glasses were cleaned in an ultrasonic bath, using distilled water and iso-propanol, and dried with dry airflow for 20 min. An ethanol solution of titanium

tetra-isoporopoxide, containing few drops of HNO_3 (pH = 2), was stirred during 24 h in argon atmosphere before using. This mixture was spin-coated on pre-cleaned FTO at 3000 rpm for 1 min. The films were then sintered at 450 °C for 1 h and cooled down to room temperature. A thick compact layer of TiO_2 of about 100 nm was obtained.

Nanoporous TiO_2 electrodes were then deposited on the compact layer by spin-coating using a TiO_2 paste (Solaronix Nanoxide-HT). Electrodes were then sintered at 450 °C for 15 min and cooled down to room temperature in the furnace. The thickness of the films on FTO substrates was determined by a Dektak profilometer (Veeco, Dektak 3) and found to be about 1.5 μm. The upper layers of the paste were soaked with $RuL_2(NCS)_2:(TBA)_2$ dye, where L is 2,2'-bipyridyl-4,4'-dicarboxylic acid and TBA is tetrabutylammonium (Solaronix), used as sensitizer for these layers. Subsequently, a hole transport layer was deposited by spin-coating from chloroform solution (10 mg in 1 ml of chloroform : [HY-CARB] = 0.016 M). The thickness of the hole transporting layer on top of the TiO_2 was typically in the range of 100–150 nm, as determined by Dektak measurements. After an additional drying step under vacuum, the gold electrode was deposited by cathodic sputtering.

The morphology of these layers was examined with an atomic force microscope (AFM) in contact mode. Diffraction patterns were measured by X-ray diffractometer (XRD) from Enraf Nonius, equipped with a copper tube.

Contactless transient photoconductance measurements in the microwave frequency range (K_α band at 30 GHz) were performed with the Time Resolved Microwave Conductivity (TRMC) technique as described previously [17] and in Fig. 2. TRMC signals were induced by 10 ns FWHM laser pulses at 355 nm with

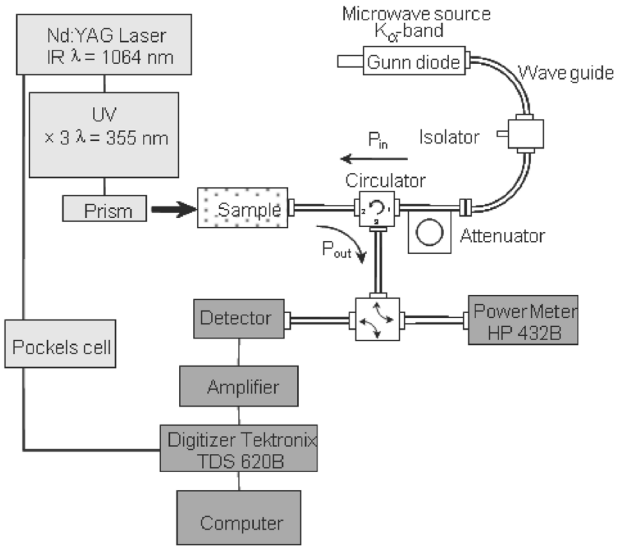

Fig. 2. Schematic representation of the Time Resolved Microwave Conductivity setup.

a Nd:YAG laser. The TRMC signal $\Delta P(t)/P$ is the relative change of the microwave power reflected by the sample, induced by a photo-induced change of the conductance $(\Delta S(t))$. It is shown that:

$$\frac{\Delta P(t)}{P} = A\Delta S(t), \tag{1}$$

where A is a constant, called the sensitivity factor. It depends on the experimental configuration and the electrical parameters of the sample. For the present work it is important to note that an increase of the conductivity of the sample leads to a decrease of A. In the extreme case of an ideal metal, $A = 0$, because microwaves cannot penetrate the sample and no TRMC signal can be detected.

As $\Delta S(t)$ is determined by the contributions of excess electrons $\Delta N(t)$ (cm^{-2}) at the bottom of the conduction band with a mobility μ_n and of excess holes $\Delta P(t)$ (cm^{-2}) at the top of the valence band with a mobility μ_p, we have

$$\frac{\Delta P(t)}{P} = A(\Delta N(t)\mu_n e + \Delta P(t)\mu_p e). \tag{2}$$

The measurement of I was made with a Keithley SM4 2400 source-meter in air, in dark and under standard AM 1.5 illumination (94 $\mathrm{mW/cm^2}$) with solar simulator Atlas Solar Constant 575 PV.

3. RESULTS AND DISCUSSION

3.1. Characterization of the TiO_2 layer

Figure 3 shows the XRD patterns of TiO_2 layers, deposited on the glass substrate and on FTO/dense TiO_2 substrate. Diffractograms have the same general characteristics revealing anatase structure of TiO_2. The appearance of only one anatase peak $(2\theta = 25.35°)$ is related to the low thickness of the dense TiO_2 layer (about 100 nm). Meanwhile, considering porous titanium dioxide, except SnO_2 peaks, all the peaks in the XRD pattern are assigned to anatase TiO_2 without any indication of other crystalline products such as rutile. Moreover, they are relatively broad due to the nanosize of the crystals; we have also roughly estimated the particle size of TiO_2 in the film equal to 30 nm, using the Debye Scherrer equation [16].

Figure 4 illustrates the surface morphology of various SnO_2:F/dense TiO_2, films as determined by atomic force microscopy in the contact mode. According to AFM images, the SnO_2:F/dense TiO_2 films show a very homogeneous surface (RMS surface roughness of approximately 2.0 ± 0.8 nm) without pores and pinholes. In contrast, Figs. 4b and c show a less smooth surface for porous nc-TiO_2 and porous nc-TiO_2/Ru-dye with RMS surface roughness of about 15 ± 2 nm and 14 ± 2 nm, respectively. Deep holes or large area defects are not detected for

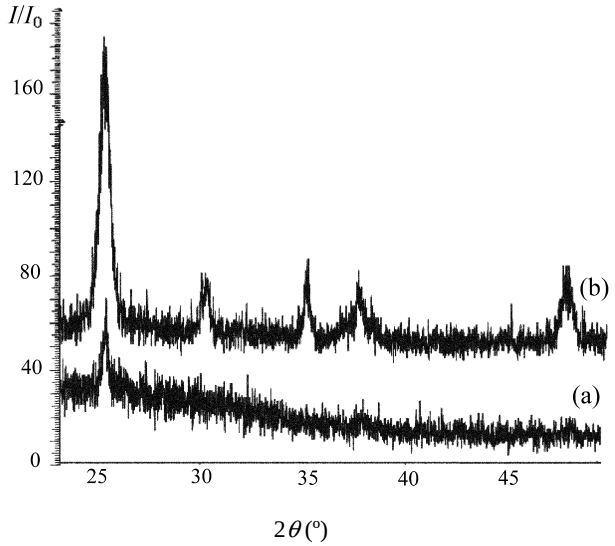

Fig. 3. X-ray diffractograms of a dense TiO_2 layer (anatase structure), elaborated by sol-gel method and coated on glass support (a) and porous nc-TiO_2 layer (Solaronix) coated on FTO/denseTiO_2 (b).

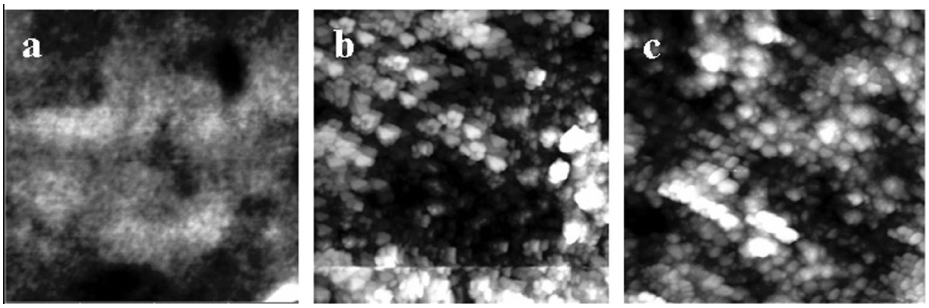

Fig. 4. AFM images (1×1 μm) of SnO_2 : F/dense TiO_2 (a), SnO_2 : F/dense TiO_2/porous nc-TiO_2 (b) and SnO_2 : F/dense TiO_2/porous nc-TiO_2/Ru-dye (c).

the Ru-dye films on top of TiO_2 and therefore shunts should not be a major problem of the photovoltaic devices. That is in good agreement with the results from *I–V* measurements.

Illumination of SnO_2 : F/TiO_2 films on glass substrates by 355 nm laser pulses leads to measurable TRMC signals (Fig. 5). The signal amplitude, i.e. the maximum height at about 10 ns for the present measurements, is proportional to the excitation density. The shape of the TRMC signal is independent of the excitation density and characterized by a non-exponential decay.

From these observations the following conclusions are drawn.

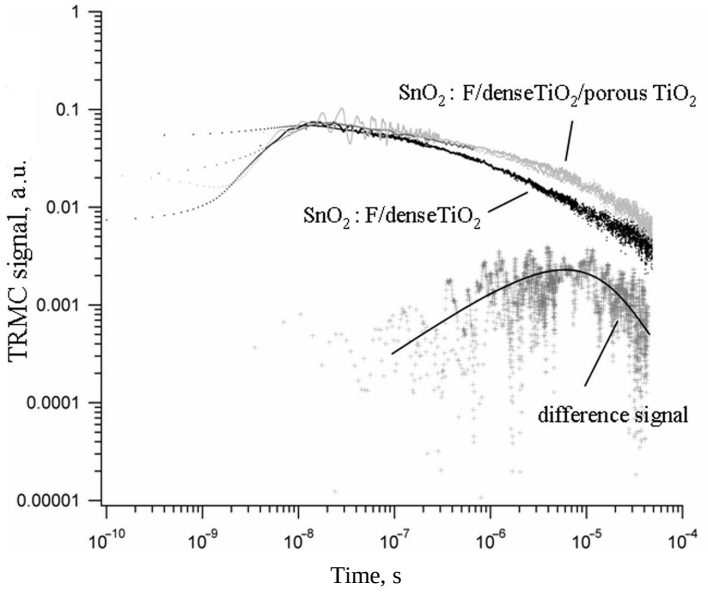

Fig. 5. TRMC signals of SnO_2:F/denseTiO_2 films on glass induced by 10 ns (FWHM) laser pulses at 355 nm in a double logarithmic representation. The black curve refers to the illumination of the SnO_2:F/denseTiO_2–air interface (front), the grey curve refers to the illumination of the SnO_2:F/denseTiO_2/porous TiO_2–air interface. The thin black curve refers to the difference signal obtained by subtraction of the signal of SnO_2:F/denseTiO_2 from the signal of the porous TiO_2 on SnO_2:F/denseTiO_2.

The signal, observed in the bare SnO_2:F/denseTiO_2/porous TiO_2 is higher than that in the SnO_2:F/denseTiO_2 (for identical conditions) after the excitation pulse (at 10 ns). Although other explanations are possible, this increase is probably due to the excess in charge carriers in a region, characterized by low mobility compared to a region, characterized by a much lower mobility. These results are analogous to the ones obtained in a-Si:H/c-Si heterojunctions [17]. In the present system, the most probable candidate for this process is the transition of an excess electron, generated in TiO_2 to the SnO_2:F. Although the data from the literature on the electron mobility in these materials in the case of a single crystalline material cannot be used, it is plausible that in TiO_2, $\mu_n << 1$ cm^2 V^{-1} s^{-1} and in SnO_2:F, $\mu_n >> 1$ cm^2 V^{-1} s^{-1}. Thus this process leads to the increase of the signal after 10 ns.

The signal in SnO_2:F (highly n doped) is due exclusively to excess electrons [17] and the injection process induces also only electrons. Thus the TRMC signals in the bare SnO_2:F/denseTiO_2 film and in the SnO_2:F/dense TiO_2/porous TiO_2 film are only due to excess electrons. As the decay behaviour in SnO_2:F/denseTiO_2 films does not depend on the excitation density, it must be identical for SnO_2:F/dense TiO_2 films and for SnO_2:F/denseTiO_2/porous TiO_2 films after the termination of the injection process (i.e. after about 1 μs). This is confirmed by the experimental results (Fig. 5).

The proportionality factor A (Eq. (1)) is not very different for excess charge carriers in TiO_2 and in $SnO_2:F$ in the present configuration. So the contribution of excess charge carriers to the TRMC signal depends mainly on their mobility. As stated above, the mobility in $SnO_2:F$ is much higher than in TiO_2; that explains why no TRMC signal is observed after generation of excess charge carriers only at the top of the TiO_2 film by illumination of the TiO_2–air interface with 355 nm light.

The signal of difference in Fig. 5 shows an increase until about 500 ns, giving way to a decrease, identical to that in the bare $SnO_2:F$/denseTiO_2 film after about 3 μs. The time of the increase of this signal is mainly due to the diffusion time of excess charge carriers in the TiO_2 to the $SnO_2:F$/denseTiO_2/porous TiO_2 interface. This process is characterized by a distribution of diffusion times due to the distribution of distances between excess charge carriers and the interface. These observations point to a band bending at the interface with an accumulation layer for electrons.

3.2. Characterization of molecular glasses

3.2.1. Thermal properties

Thermal properties of different molecules CARB-I-EDOT, CARB-I-CARB and HY-CARB have been studied by Differential Scanning Calorimetry (DSC) (Fig. 6). During the first heating scan, we observe for the three molecules melting temperatures 175 °C, 132 °C and 110 °C, respectively, for the two imines structures and for the hydrazone one (Table 1). After cooling, followed by a second heating scan, we clearly observe the appearance of glass transition at 62 °C for CARB-I-EDOT, at 72 °C for CARB-I-CARB and at 76 °C for HY-CARB, indicating that the material is in a amorphous state and that the molecules can be considered as molecular glasses. The ability of such a molecule of low molecular weight to stay amorphous in a metastable state allows the realization of a thin film with good

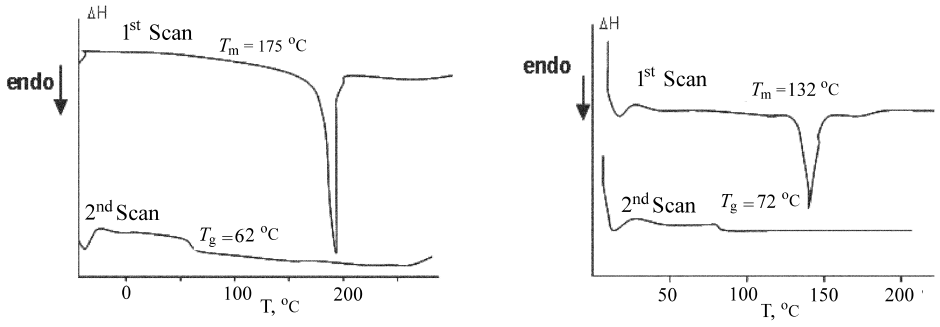

Fig. 6. Example of the thermal behaviour of CARB-I EDOT (a) and CAR-I-CARB (b) during two consecutive heating scans.

Table 1. Physico-chemical properties of different molecular glasses

	T_m, °C	T_g, °C	λ_{max}, nm	Optical gap, eV	HOMO*, eV
HY-CARB	110	76	356	3.1	–4.76
CARB-I-CARB	132	72	349 and 375	2.5	–5.10
CARB-I-EDOT	175	62	362 and 386	2.82	–5.25

* Evaluated by electropolymerization.

contact with the nanostructured inorganic layer. For comparison, the dimer of N-ethylcarbazole possesses a glass temperature at 79 °C [18].

3.2.2. Optical characterization

The maximal absorbance of HY-CARB in chloroform solution occurs at $\lambda_{max} = 356$ nm (Fig. 7), which is red-shifted in comparison with bis(N-hexyl-carbazole). It is likely that hydrazone groups participate in the electronic delocalisation of π-electrons, which is more important than the one limited to two nitrogen atoms, as usually described for the unsubstituted dimer. From the onset of the absorption band, it is possible to evaluate the optical bandgap of the molecule. We obtain a value of 3.1 eV, which is more than 0.7 eV lower than the one of the unsubstituted dimer.

Figure 7 shows also the absorption spectrum of the two molecules, containing imine groups. As shown in Table 1, two absorption bands can be observed at 362 and 386 nm for CARB-I-EDOT and at 349 and 375 nm for CARB-I-CARB, indicating a large electronic delocalization due to the conjugation of the structure via the imine bridge. The optical bandgaps are evaluated at 2.82 eV and 2.50 eV, respectively. For all the structures, the absorption spectrums are blue-shifted in comparison with the absorption band of the ruthenium dye. Thus, molecular glasses will not absorb the light, allowing the generation of charge carriers via the sensitizer.

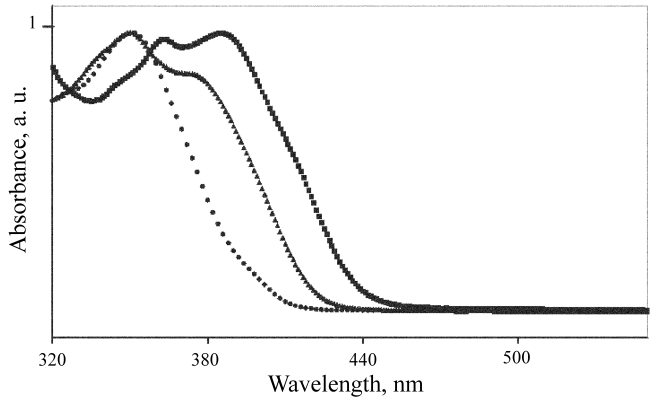

Fig. 7. Spectres: ■ CARB-I-EDOT; ▲ CARB-I-CARB; ● HY-CARB (in chloroform).

3.2.3. Electrochemical characterization

Figure 8 shows the electrochemical characterization of thin films of the three molecules deposited onto a Pt electrode by spin coating. Electrochemical behaviour of HY-CARB is very similar to the one observed for unsubstituted carbazole dimers. Indeed, during cyclic voltammogram at 50 mV/s in $CH_3CN/LiClO_4$ 0.1 M, two well defined anodic processes are observed at Epa_1 = 0.62 V/SCE and Epa_2 = 1.13 V/SCE, which can be attributed to the successive oxidation of the molecule into cation radical and dication [19].

On the reverse scan, reduction of peaks at 1.00 and 0.49 V/SCE (Fig. 8c) indicate good stability of different oxidized states of the molecules. As already observed with UV-Visible spectroscopy, hydrazone substituents increase the conjugation of the dimer structure and thus lead to a decrease of the oxidability of the molecule in comparison with the biscarbazole. The oxidation potential is decreased for 0.35 V. Thus the presence of hydrazone allows improving the donor properties of biscarbazole by increasing its HOMO energy level. As already described in [20], it is possible to approximate its value from the E_{onset} of the oxidative current of the voltammogram. We obtained a value close to –4.76 eV.

The electroactivity of the two other molecular glasses CARB-I-EDOT (Fig. 8a) and CARB-I-CARB (Fig. 8b), deposited and investigated in the same experimental conditions as described above, shows during oxidation a non-reversible anodic current and the E_{onset} occurs at 0.85 and 0.7 V/SCE. During the reverse scan we do

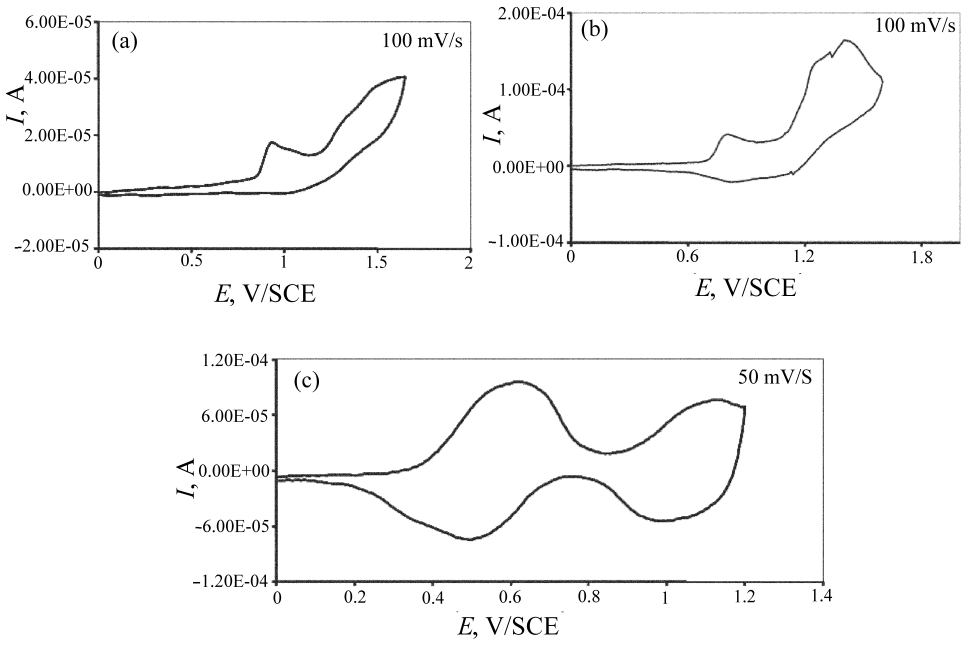

Fig. 8. Cyclic voltametry of thin films, deposited onto Pt (Φ = 1 cm) electrode in CH_3CN-$LiClO_4$ 0.1 M: CARB-I-CARB (a); CARB-I-EDOT (b); HY-CARB (c).

not see any reduction peaks, which indicates the high reactivity of the oxidative species with probably coupling reactions on the carbazole or on EDOT. By repeated scanning potentials in the potential range of the electroactive imines, we observe the formation of new redox systems, occuring at a lower potential than that of the immine molecule and whose intensities increase during cycling. This behaviour is characteristic for electropolymerization of the monomers and confirms the reactivity of the cation radical. The HOMO energetic level of the two imines are evaluated at –5.1 eV for CARB-I-CARB and –5.25 eV for CARB-I-EDOT.

3.3. Solar cell device

The solar cell was produced in sandwich geometry between two metal electrodes with different work functions (SnO_2 : F : 4.7 eV and Au 5.1–5.4 eV). In the present configuration we have chosen gold as the top electrode material, because its work function is close to the highest occupied molecular orbital (HOMO) of the hole conductor HY-CARB. Thus hole injection from the molecular glass into the metal electrode is energetically possible. In such device configuration, the TiO_2 conduction band electrons and the holes in the molecular glass are subsequently transported to the contact electrodes and the dye is regenerated by the hole injection into the molecular glass. Figure 9 shows a schematic energy diagram of SnO_2 : F/nc-TiO_2/Ru-dye/HY-CARB/Au three-layered devices.

The I/V characteristics for a device are presented in Fig. 10. Typical data of this device under standard AM 1.5 illumination with 94 mW/cm^2 are: $V_{OC} \cong 230$ mV and FF = 0.29.

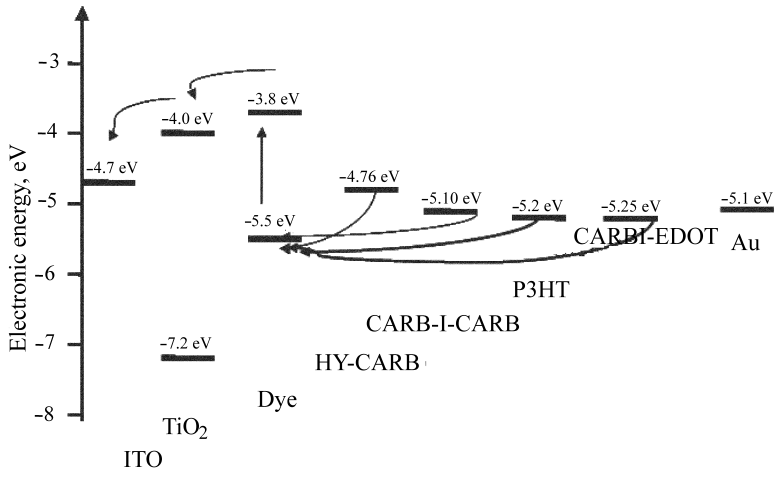

Fig. 9. Schematic energy diagram of SnO_2 : F/nc-TiO_2/Ru-dye/molecular glasses/Au.

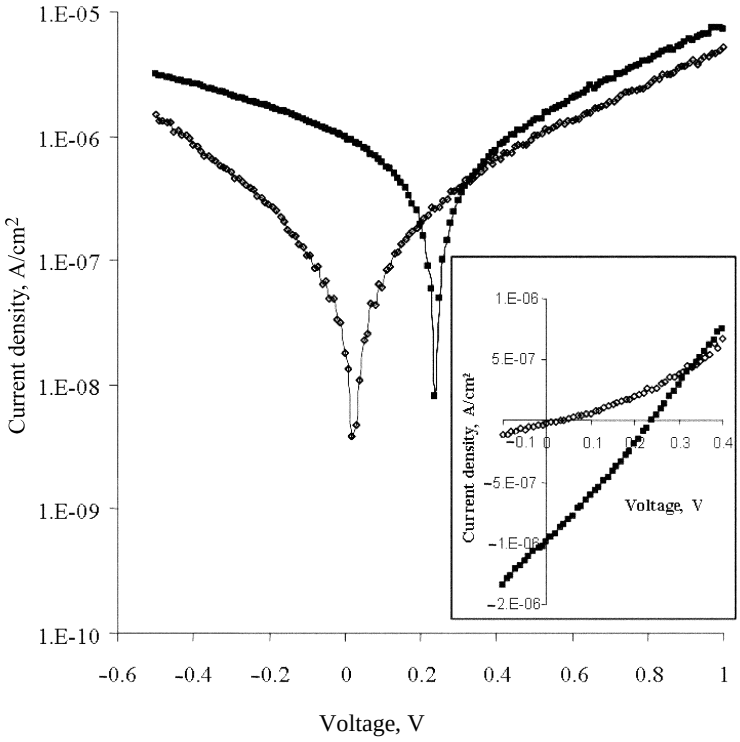

Fig. 10. I/V characteristics of a SnO_2:F/nc-TiO_2/Ru-dye/HY-CARB/Au hybrid solar cell; open squares – dark; solid squares – illuminated under standard AM 1.5 illumination (94 mW/cm^2); the inset is a linear plot of the I/V data for positive voltage.

4. CONCLUSIONS

New molecular glasses, based on carbazole and 3,4-ethylenedioxythiophene, have been synthesized and characterized. The amorphous properties have been determined by thermal analysis. The glass temperature of each molecule is much higher than the ambient temperature. The electronic delocalization of the imine or hydrazone group allows adjusting the HOMO level higher than the one of the sensitizer and close to the Fermi level of the electrode. A typical solid state dye sensitizer solar cell has been realized with HY-CARB molecular glass with low photocurrent. Work is in progress to study the possibility of doping the molecular glass to improve the charge motilities. We have also applied the TRMC technique to study photoinduced charge separation in bare SnO_2:F/denseTiO_2 and SnO_2:F/denseTiO_2/porous TiO_2 films. This technique enables one to determine the key parameters of photovoltaic materials such as charge separation efficiency and decay kinetics in the absence of electrodes and electrolyte.

REFERENCES

1. Nazeeruddin, M. K., Kay, A., Rodicio, I., Humphry-Baker, R., Muller, E., Liska, P., Vlachopoulos, N. and Gratzel, M. Conversion of light to electricity by cis-X_2bis(2,2'-bipyridyl-4,4'-dicarboxylate)ruthenium(II) charge-transfer sensitizers ($X = Cl^-$, Br^-, I^-, CN^-, and SCN^-) on nanocrystalline titanium dioxide electrodes. *J. Am. Chem. Soc.*, 1993, **115**, 6382–6390.
2. Barbe, C. J., Arendse, F., Comte, P., Jirousek, M., Lenzmann, F., Shklover, V. and Gratzel, M. Nanocrystalline titanium oxide electrodes for photovoltaic applications. *J. Am. Ceram. Soc.*, 1997, **80**, 3157–3171.
3. Green, M. A., Emery, K., Bucher, K., King, D. L. and Igari, S. Solar cell efficiency tables (version 11). *Prog. Photovolt. Res. Appl.*, 1998, **6**, 35–42.
4. Cao, F., Oskam, G. and Searson, P. C. Electrical and optical properties of porous nanocrystalline TiO_2 films. *J. Phys. Chem.*, 1995, **99**, 17071–17073.
5. Tennakone, K., Kumara, G. R. R. A., Kumarasinghe, A. R., Wijayantha, K. G. U. and Sirimanne, P. M. A dye-sensitized nano-porous solid-state photovoltaic cell. *Sci. Technol.*, 1995, **10**, 1689–1693.
6. Tennakone, K., Kumara, G. R. R. A., Kottegoda, I. R. M., Wijayantha, K. G. U. and Perera, V. P. S. A solid-state photovoltaic cell sensitized with a ruthenium bipyridyl complex. *J. Phys. D: Appl. Phys.*, 1998, **31**, 1492–1496.
7. O'Regan, B. and Schwartz, D. T. Efficient photo-hole injection from adsorbed cyanine dyes into electrodeposited copper(I) thiocyanate thin films. *Chem. Mater.*, 1995, **7**, 1349–1355.
8. Hagen, J., Schaffrath, W., Otschik, P., Fink, R., Bacher, A., Schmidt, H.-W. and Haarer, D. Novel hybrid solar cells consisting of inorganic nanoparticles and an organic hole transport material. *Synth. Met.*, 1997, **89**, 215–220.
9. Murakoshi, K., Kogure, R., Wada, Y. and Yanagida, S. Solid state dye-sensitized TiO_2 solar cell with polypyrrole as hole transport layer. *Chem. Lett.*, 1997, **5**, 471–472.
10. Bach, U., Lupo, D., Comte, P., Moser, J. E., Weissortel, F., Salbeck, J., Spreitzer, H. and Gratzel, M. Solid-state dye-sensitized mesoporous TiO_2 solar cells with high photon-to-electron conversion efficiencies. *Nature*, 1998, **395**, 583–585.
11. Gebeyehu, D., Brabec, C. J., Vangeneugden, D., Kiebooms, R., Vanderzande, D., Kienberger, F., Schindler, H. and Sariciftci, N. S. The interplay of efficiency and morphology in photovoltaic devices based on interpenetrating networks of conjugated polymers with fullerenes. *Synth. Met.*, 2001, **125**, 279–287.
12. Sariciftci, N. S., Smilowitz, L., Heeger, A. J. and Wudl, F. Photoinduced electron transfer from conducting polymer to buckminsterfullerene. *Science*, 1992, **258**, 1474–1476.
13. Sariciftci, N. S. and Heeger, A. J. In *Handbook of Organic Conductive Molecules and Polymers*, vol. 1 (Nalwa, H. S., ed.). J. Wiley, New York, 1997, 437–455.
14. Grazulevicius, J. V., Strohriegl, P., Pielichowski, J. and Pielichowski, K. Carbazole-containing polymers: synthesis, properties and applications. *Prog. Polym. Sci.*, 2003, **28**, 1297–1353.
15. Michalevičiūtė, A., Buika, G., Ostrauskaitė, J., Gražulevičius, J. V., Jankauskas, V., Tran-Van, F. and Chevrot, C. Glass-forming 3,3'-bicarbazyl-based dihydrazones. *Environ. Chem. Phys.*, 2004, **26**, 174–177.
16. Azaroff, L. B. *The Powder Method*. McGraw-Hill, New York, 1958.
17. Kunst, M., Neitzert, H. C. and Sanders, A. Characterization of InP and GaAs films by contactless transient photoconductivity measurements. *Thin Solid Films*, 2004, **450**, 159–162.
18. Lideikis, E., Grigalevicius, S., Grazulevicius, J. V., Gaidelis, V., Antulis, J., Jankauskas, V., Tran-Van, F. and Chevrot, C. Synthesis and properties of the polymers containing 3,3'-bicarbazole units in the main chain and their model compounds. *Polymer*, 2002, **43**, 5693–5697.
19. Tran-Van, F., Henri, T. and Chevrot, C. Synthesis and electrochemical properties of mixed ionic and electronic modified polycarbazole. *Electrochim. Acta*, 2002, **47**, 2927–5936.

20. de Leeuw, D. M., Simenon, M. M. J., Brown, A. R. and Einerhand, R. E. F. Stability of n-type doped conducting polymers and consequences for polymeric microelectronic devices. *Synth. Met.*, 1997, **87**, 53–59.

Molekulaarklaasidel põhinevate tahkete hübriidpäikesepatareide uurimine

Fabrice Goubard, Reda Aîch, François Tran-Van, Asta Michaleviciute, Franck Wünsch, Marinus Kunst, Josas Grazulevicius, Bernard Ratier ja Claude Chevrot

On sünteesitud molekulaarklaasidel põhinevad hüdrasoon- ja imiinrühmadega karbasooli ja etüleendioksütiofeeni derivaadid. Termiline analüüs kinnitab saadud molekulide metastabiilseid amorfseid omadusi. On uuritud nende ühendite elektrokeemilisi omadusi ja näidatud hüdrasoon- ja imiinrühmade konjugatsiooniefekti struktuuride elektroonsele delokalisatsioonile. Uurimuse tulemused näitavad, et sellised molekulaarklaasid võiksid leida kasutamist fotogalvaanilistes seadistes.